Singlet Oxygen–mediated Protein Oxidation: Evidence for the Formation of Reactive Side Chain Peroxides on Tyrosine Residues

Author(s): Adam Wright, William A. Bubb, Clare L. Hawkins, and Michael J. Davies
Source: Photochemistry and Photobiology, 76(1):35-46.
Published By: American Society for Photobiology
DOI: http://dx.doi.org/10.1562/0031-8655(2002)076<0035:SOMPOE>2.0.CO;2
URL: http://www.bioone.org/doi/full/10.1562/0031-8655%282002%29076%3C0035%3ASOMPOE%3E2.0.CO%3B2

Photochemistry and Photobiology, 2002, 76(1): 35–46

Singlet Oxygen–mediated Protein Oxidation: Evidence for the Formation of Reactive Side Chain Peroxides on Tyrosine Residues¶

Adam Wright[1], William A. Bubb[2], Clare L. Hawkins[1] and Michael J. Davies*[1]

[1]EPR Group, Heart Research Institute, Sydney, Australia and [2]Department of Biochemistry, University of Sydney, Sydney, Australia

Received 17 December 2001; accepted 15 April 2002

ABSTRACT

Singlet oxygen ($^1O_2$) is generated by a number of enzymes as well as by UV or visible light in the presence of a sensitizer and has been proposed as a damaging agent in a number of pathologies including cataract, sunburn, and skin cancers. Proteins, and Cys, Met, Trp, Tyr and His side chains in particular, are major targets for $^1O_2$ as a result of their abundance and high rate constants for reaction. In this study it is shown that long-lived peroxides are formed on free Tyr, Tyr residues in peptides and proteins, and model compounds on exposure to $^1O_2$ generated by both photochemical and chemical methods. The yield of these species is significantly enhanced in D_2O and decreased by azide. Nuclear magnetic resonance and mass spectroscopic analysis of reaction mixtures, or materials separated by high-performance liquid chromatography, are consistent with the initial formation of an (undetected) endoperoxide that undergoes rapid ring-opening to give a hydroperoxide situated at the C1 ring-position (*i.e.* para to the phenolic group). In the presence of a free α-amino group (*e.g.* with free Tyr), rapid ring-closure occurs to give an indolic hydroperoxide that decays into the corresponding alcohol, 3a-hydroxy-6-oxo-2,3,3a,6,7,7a-hexahydro-1*H*-indole-2-carboxylic acid. Hydroperoxides that lack a free α-amino group (*e.g.* those formed on 3-(4-hydroxyphenyl)propionic acid, *N*-Ac-Tyr and Tyr-containing peptides) are longer-lived, with half-lives of hours to days. These species undergo slow decay at low temperatures to give the corresponding alcohol. Their rate of decay is enhanced at 37°C, or on exposure to UV light or metal ions, and gives rise to reactive radicals, *via* cleavage of the peroxide bond. These radicals have been characterized by electron paramagnetic resonance spin trapping. These studies demonstrate that long-lived Tyr-derived peroxides are formed on proteins exposed to $^1O_2$ and that these may promote damage to other targets *via* further radical generation.

INTRODUCTION

Singlet oxygen (molecular oxygen in its $^1\Delta_g$ state; $^1O_2$) is known to be produced in a number of heme protein– and lipoxygenase-catalyzed reactions (*e.g.* reactions involving myelo-, lacto-, chloro- and eosinophil-peroxidases [1–3]). $^1O_2$ generation has also been detected with a number of cell types, including stimulated neutrophils, eosinophils and macrophages (4–6). UV exposure can generate $^1O_2$, as does visible light in the presence of suitable (exogenous or endogenous) sensitizers (7). $^1O_2$ is also formed during dimerization reactions of peroxyl radicals, *via* the Russell mechanism, and hence is a common intermediate in many peroxidation reactions (8). $^1O_2$ reacts with a broad spectrum of biological molecules including DNA, cholesterol, lipids, and amino acids and proteins (9), and it has been postulated that damage caused thereby plays a role in the development of cataract, sunburn and some skin cancers (10,11).

Proteins are major biological targets for $^1O_2$ because of their abundance and high rate constants for reaction (9,12). The interaction of $^1O_2$ with amino acids, peptides and proteins can occur *via* two different mechanisms: chemical reaction and physical quenching. Of the common amino acids, only Trp residues give rise to significant levels of physical quenching (*cf.* rate constants of *ca* $2–5 \times 10^7$ and 3×10^7 $dm^3\ mol^{-1}\ s^{-1}$ for physical and chemical reaction, respectively [13]). Reaction with all other amino acid side chains occurs primarily by chemical reaction (reviewed in [9,12,14]). Five common amino acid side chains undergo rapid chemical reaction with $^1O_2$ at physiological pH values: His (k *ca* 3.2×10^7 $dm^3\ mol^{-1}\ s^{-1}$ at pH 7.1, though this value is markedly pH-dependent); Trp (k 3×10^7 $dm^3\ mol^{-1}\ s^{-1}$); Tyr (k 0.8×10^7 $dm^3\ mol^{-1}\ s^{-1}$); Met (k 1.6×10^7 $dm^3\ mol^{-1}\ s^{-1}$); and Cys (k 8.9×10^6 $dm^3\ mol^{-1}\ s^{-1}$) (15). All other side chains react with $k < 0.7 \times 10^7$ $dm^3\ mol^{-1}\ s^{-1}$ (15). At high pH values, where there is a significant con-

¶Posted on the web site on 3 May 2002.

*To whom correspondence should be addressed at: The Heart Research Institute, 145 Missenden Road, Camperdown, Sydney, NSW 2050, Australia. Fax: 612-9550-3302; e-mail: m.davies@hri.org.au

Abbreviations: BSA, bovine serum albumin; DMPO, 5,5-dimethyl-1-pyrroline-*N*-oxide; DOPA, 3,4-dihydroxyphenylalanine; EDTA, ethylenediamine-tetraacetic acid; EPR, electron paramagnetic resonance; ESI-MS, electrospray ionization–mass spectrometry; HOHICA, 3a-hydroxy-6-oxo-2,3,3a,6,7,7a-hexahydro-1*H*-indole-2-carboxylic acid; HMBC, heteronuclear multiple bond correlation; HPLC, high-performance liquid chromatography; HPPA, 3-(4-hydroxyphenyl)propionic acid; HSQC, heteronuclear single quantum coherence; MNP, 2-methyl-2-nitrosopropane; NMR, nuclear magnetic resonance; $^1O_2$, singlet oxygen; ODS, octadecyl-silanized silica; RB, rose bengal.

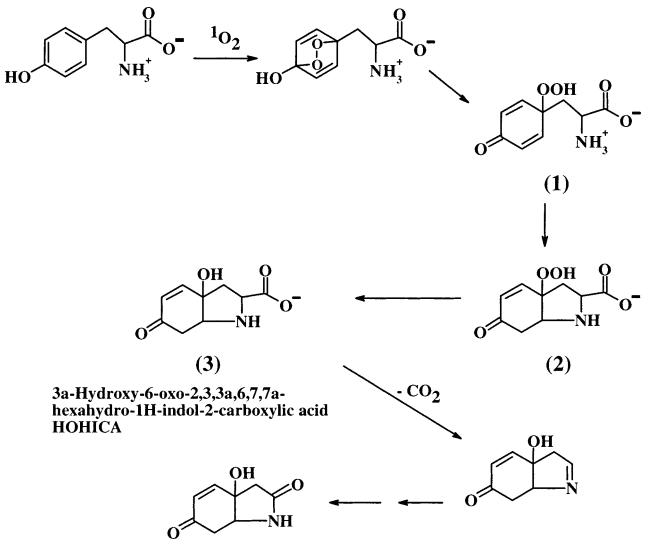

Scheme 1.

centration of the unprotonated (neutral) form, Arg and Lys residues also undergo photooxidation (16). Previous studies have shown Tyr, His, and Trp residues, and related materials yield semistable peroxidic species on reaction with $^1O_2$ (reviewed in [9,12]), though the exact nature of some of these species is unknown. In the case of Tyr it has been proposed that oxidation occurs *via* the reactions shown in Scheme 1 (17–19).

$^1O_2$-mediated protein oxidation can give rise to a range of biological consequences including oxidation of side chains, backbone fragmentation (though this is a minor process with most proteins), dimerization or aggregation, unfolding or conformational changes, and alteration in cellular handling and turnover (reviewed in [9,12]). In some cases, such as the cataractous lens, evidence has been presented for the occurrence of these reactions *in vivo*, and for a role played by such oxidation in the etiology of the disease (20). Although many of these effects may arise *via* direct $^1O_2$-mediated oxidation of the target, ''dark'' reactions (*i.e.* reactions that occur after the cessation of exposure to $^1O_2$) can also play a role. These processes consume other amino acids, in addition to those discussed in the foregoing (*e.g.* [21,22]), and can give rise to cross-links (9).

Some of the biological consequences of $^1O_2$-mediated protein oxidation may arise from the formation and subsequent reactions of reactive peroxides such as (**1**) and (**2**). In support of this hypothesis, it has been shown that photooxidized peptides and proteins can inhibit key cellular enzymes *via* processes that involve protein and peptide peroxides (23). It has also been established that peroxides generated by γ-radiation can bring about depletion of cellular reducing equivalents and antioxidants (24), inhibition of cellular enzymes (25), and induce DNA damage (26–28). Further evidence for the potential importance of peroxides in photooxidative damage arises from studies on lenses, which have shown that glutathione (GSH) peroxidase-mimics that remove peroxides can prevent photooxidative damage and the continued thiol loss that occurs after cessation of light exposure (29).

As a result of the potential role of $^1O_2$-generated protein and peptide peroxides in photooxidative damage induced by $^1O_2$, a detailed study has been carried out on the nature, and further reactions, of peroxides formed on photooxidized free Tyr, and Tyr residues in peptides and proteins.

MATERIALS AND METHODS

Materials. L-Tyr, 3-(4-hydroxyphenyl)propionic acid (HPPA), *N*-acetyl Tyr, Gly-Gly-Gly, bovine serum albumin (BSA), sodium molybdate and xylenol orange were from Sigma (St. Louis, MO). Hydrogen peroxide (30%) was from BDH (Poole, Dorset, UK). Deuterium oxide, rose bengal (RB), MNP (2-methyl-2-nitrosopropane) were from Aldrich (Castle Hill, New South Wales, Australia). (3,5-ring-d_2)-Tyr and C(3)-d_2-Tyr were from CDN (Quebec, Canada). (2,3,5,6-ring-d_4)-Tyr was from Cambridge Isotope Labs (Andover, MA). Gly-Tyr-Gly was from Bachem (Bubendorf, Switzerland). All chemicals were used as supplied with the exception of 5,5-dimethyl-1-pyrroline-*N*-oxide (DMPO; Sigma), which was purified before use by treatment with activated charcoal. All other chemicals were of the highest grade commercially available. Water used in all experiments was passed through a four-stage Milli Q system equipped with a 0.2 μm pore size final filter. Solutions of Fe^{2+}–ethylenediaminetetraacetic acid (EDTA) (1:1 complex) were prepared using deoxygenated water and maintained under an atmosphere of oxygen-free N_2 during use.

Photochemical $^1O_2$ formation. Solutions of Tyr, HPPA, *N*-acetyl Tyr, Gly-Tyr-Gly (all 2.5 m*M*) and BSA (75 μ*M*) were prepared in water or deuterium oxide at pH or pD values of *ca* 7 and contained 10 μ*M* RB where stated. The solutions were neutralized, when necessary, with NaOH. Solutions were photolyzed, at a distance of 5 cm, using light from a Kodak S-AV 2050 slide projector (250 W bulb) filtered through a 345 nm cutoff filter. Samples were gassed continually during the photolysis period with compressed air or O_2 and maintained at 4°C. In experiments using sodium azide, this chemical was added to give a concentration of 5 m*M*. All samples were treated postphotolysis with catalase (3150 units mL^{-1}, 10 min, 22°C) to remove photogenerated H_2O_2. This treatment does not affect the yield of organic peroxides (23).

Molybdate-catalyzed production of $^1O_2$. Solutions of Tyr and Gly-Tyr-Gly (both 2.5 m*M*) were prepared in water containing Na_2MoO_4 (12.5 m*M*). Aliquots of 30% H_2O_2 were added at 0, 1 and 10 min to give a final H_2O_2 concentration of 0.31 *M* and the reaction allowed to proceed for 30 min.

Peroxide determinations. Peroxide concentrations were determined using a modified ferric-xylenol orange (FOX) assay with H_2O_2 standards (30). The thermal stability of the Tyr-derived and related peroxides was investigated by incubating photolyzed solutions of Tyr or related parent compounds at 4, 22 and 37°C in the absence of light. Aliquots were removed at the stated time points and residual peroxide concentrations determined. The stability of Tyr-derived peroxides to reductants was examined by treating samples with Fe^{2+}–EDTA (1:1 complex) or $NaBH_4$ (both 200 μ*M* final concentration) and incubating for 60 min at 4°C before assay of residual peroxides. In the Fe^{2+}–EDTA experiments a small quantity of Chelex resin was added postincubation to remove the Fe^{2+}. The stability of preformed peroxides to visible and UV light was investigated using samples where the RB was removed by passage through an Acrodisc Syringe Filter (Pall Gelman, Ann Arbor, MI) with a 0.2 μm Supor membrane; RB binds readily to such membranes. Removal of the sensitizer was confirmed by visible spectroscopy. The treated solutions were subsequently photolyzed using either a visible light source (as in the previous) or with a broad-spectrum 150 W mercury–xenon UV lamp, and residual peroxide levels determined at the stated time points.

Electron paramagnetic resonance spectroscopy. Electron paramagnetic resonance (EPR) spectra were recorded at room temperature using a Bruker EMX X-band spectrometer equipped with 100 kHz modulation and a cylindrical ER4103 TM cavity. Samples were contained in a flattened aqueous sample cell. Spectral accumulations were initiated within 2 min of sample preparation unless stated otherwise. Hyperfine couplings were measured directly from the field scan and confirmed by spectral simulation using the WINSIM program. Typical spectrometer parameters were as follows: gain 1×10^6, modulation amplitude 0.05–0.1 mT, time constant 0.16 s, scan

time 84 s, microwave power 32 mW, resolution 1024 points and frequency 9.76 GHz, with four scans averaged.

High-performance liquid chromatography separations. High-performance liquid chromatography (HPLC) analyses were performed on a Shimadzu (Rydalmere, New South Wales, Australia) system running Shimadzu Class VP software. A reverse phase Zorbax column (25 cm × 4.6 mm, maintained at 30°C; Agilent, Forest Hill, Victoria, Australia) packed with octadecylsilanized silica (ODS), equipped with a Pelliguard guard column (2 cm; Supelco, Castle Hill, New South Wales, Australia) was used. Injections were made using a SIL 10AD VP autoinjector. Samples were eluted at a flow rate of 1 mL min^{-1} using Shimadzu LC-10AT VP pumps, and the eluent monitored with a diode array detector (Shimadzu SPD-M10A VP) over the range 200–370 nm. The mobile phases employed were water (for free Tyr and Gly-Tyr-Gly), 0.1% trifluoroacetic acid (TFA) (for HPPA), 100 m*M* sodium perchlorate in 10 m*M* sodium phosphate buffer at pH 2.5, or 80% methanol in water. Fraction collection was on the basis of retention time and UV absorbance. Tyr concentrations were determined by comparison of peak areas with standards.

Electrospray ionization–mass spectrometry. Electrospray ionization–mass spectrometry (ESI-MS) was performed on a VG Platform instrument (VG Biotech, Altrincham, UK). Data were acquired using MassLynx software (version 3.3). Samples were dissolved in 50% aqueous methanol–1% formic acid. Solvent was delivered by a Phoenix (Fisons, Blackburn, Victoria, Australia) syringe pump at a flow rate of 10 μL min^{-1}. Two 25 μL injections were made for each analysis. Dry N_2 bath gas at atmospheric pressure was used in the evaporation of the electrospray droplets. The probe tip was set at 3.5 kV with 0.5 kV on the chicane counter electrode. The sampling cone was set at either 25 or 50 V.

Nuclear magnetic resonance spectroscopy. Spectra were recorded at a ^1H frequency of 600.14 MHz on a Bruker Avance-600 nuclear magnetic resonance (NMR) spectrometer with either a triple-resonance inverse-detection probe or a broadband inverse-detection probe, both with a triple-axis field-gradient coil. The variable temperature unit was set at 20°C; for Gly-Tyr-Gly reaction mixtures; experiments were also conducted with the variable temperature unit set to 5°C. Chemical shifts are expressed relative to internal sodium 2,2-dimethyl-2-silapentane sulfonate and generally represent the midpoints of cross-peaks in heteronuclear single quantum coherence (HSQC) spectra for protonated carbons and the midpoints of cross-peaks in heteronuclear multiple bond correlation (HMBC) experiments for nonprotonated carbons. All resonance assignments were supported by correlation spectroscopy (COSPY), total correlation spectroscopy (TOCSY), heteronuclear single quantum coherence (HSQC), heteronuclear multiple bond correlation (HMBC) and nuclear overhauser enhancement spectroscopy (NOESY) data. Standard Bruker (XWIN-NMR version 2.6) pulse programs were used without modification, except for the NOESY experiments in which the mixing time (600 ms) incorporated either off-resonance presaturation or a low power z-gradient pulse. HSQC spectra were optimized for $^1J_{C,H}$ of 145 Hz, except for one additional experiment with the Gly-Tyr-Gly reaction mixture, which was optimized for $^1J_{C,H}$ of 155 Hz; HMBC spectra were optimized for $^nJ_{C,H}$ of 6.25 Hz. Molecular models were constructed from straws of proportionate length (Cochranes, Oxford, UK) and in Chem3D (CambridgeSoft Corporation, Cambridge, MA).

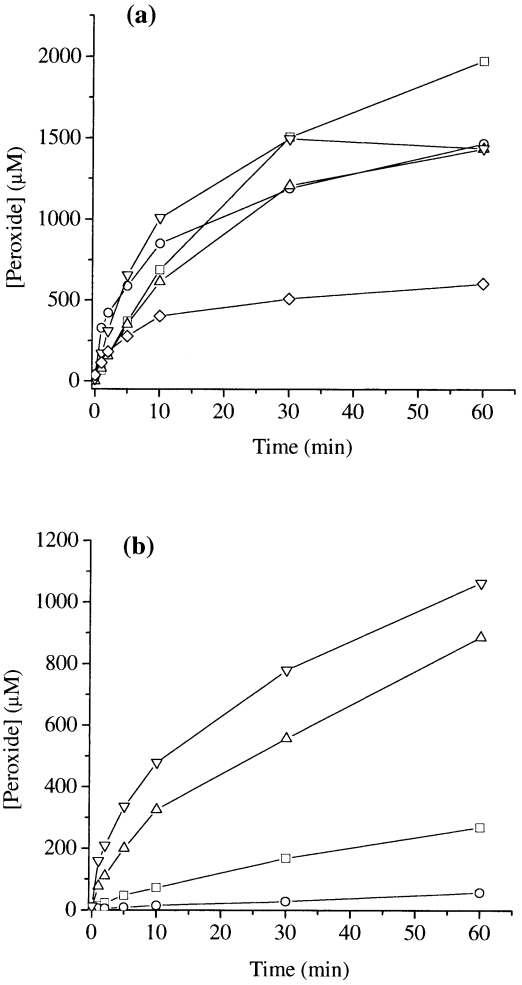

Figure 1. (a) Yields of peroxides formed on photolysis of Tyr (○), HPPA (□), *N*-acetyl Tyr (△), Gly-Tyr-Gly (▽) (all 2.5 m*M* in D_2O, pH 7) and BSA (◇) (75 μ*M* in D_2O, pH 7) by visible light in the presence of O_2 and the sensitizer RB (10 μ*M*). Photolyses were carried out, with constant air bubbling at 4°C, with visible light (λ > 345 nm). Before peroxide analysis, samples were treated with catalase (3150 units mL^{-1}, 10 min, 22°C) to remove any photogenerated H_2O_2. Peroxide concentrations were determined with a modified FOX assay (see Materials and Methods). Data are from a single experiment representative of several, each of which showed the same trend, though the absolute peroxide concentrations varied between experiments because of slight differences in the oxygenation rate. (b) Yields of peroxides formed on photolysis of Tyr in the presence of sodium azide (○) (5 m*M*), water (□), D_2O (△) or D_2O under a 100% oxygen atmosphere (▽). Data are from a single experiment representative of several.

RESULTS

Photochemical generation of peroxides

Photolysis of solutions of free Tyr, *N*-Ac-Tyr, HPPA, Gly-Tyr-Gly (each 2.5 m*M*) and BSA (75 μ*M*) at pH 7 with visible light (λ > 345 nm) in the presence of 10 μ*M* RB and O_2 resulted in the formation of peroxides as determined by the FOX assay. Because all samples were pretreated with catalase (to remove any photogenerated H_2O_2) before assay, these peroxides are ascribed to substrate-derived materials. The concentration of generated peroxides increased with photolysis time over the range investigated (Fig. 1a). Control samples photolyzed in the absence of RB or O_2 gave minimal peroxide concentrations (<2 μ*M*), as did experiments where Gly-Gly-Gly (2.5 m*M*) was photolyzed in the presence of RB and O_2. No peroxides were detected in nonphotolyzed solutions containing all the reactants. Experiments carried out in D_2O resulted in an *ca* five-fold increase in peroxide yield, whereas the inclusion of azide (5 m*M*) led to a marked decrease (Fig. 1b). Photolysis under a 100% O_2 atmosphere resulted in a 20% increase in peroxide yield (Fig. 1b). As D_2O significantly increases the lifetime of $^1O_2$, and azide ions are potent scavengers of this oxidant, these

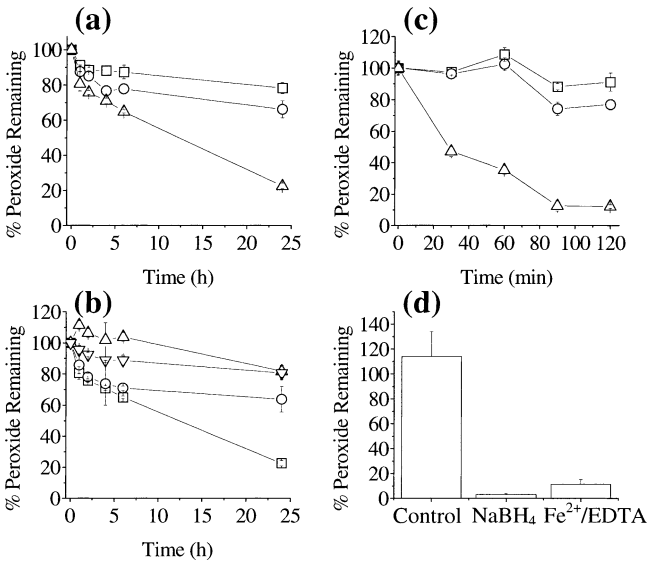

Figure 2. Decomposition of $^1O_2$-mediated peroxides. Peroxides were generated and assayed as outlined in Fig. 1. (a) Tyr-peroxides incubated at 4 (□), 26 (○), and 37°C (△) over 24 h. (b) Peroxides derived from Tyr (□), *N*-acetyl Tyr (△), HPPA (▽) and Gly-Tyr-Gly (○) incubated at 37°C over 24 h. (c) Tyr-derived peroxides, which, after removal of RB by filtration (see Materials and Methods), were incubated at 4°C in the absence of light (□) or exposed to visible light (○) (250 W lamp, $\lambda > 345$ nm) or broad-spectrum UV light (△) (150 W mercury–xenon UV lamp). (d) Tyr-derived peroxides treated with Fe^{2+}–EDTA (200 μ*M*, 1:1 complex) or $NaBH_4$ (200 μ*M*) for 1 h at 4°C. Values are expressed as a percentage of initial peroxide concentration and are means of duplicate determinations from two separate experiments (±standard deviation).

results strongly suggest that the peroxides detected arise *via* $^1O_2$-dependent processes.

Thermal stability of peroxides

The rate of thermal peroxide decay was studied at 4, 26 and 37°C over 24 h in the absence of light. Decay was most rapid at 37°C and slower at lower temperatures (Fig. 2a). Comparison of the decay rate of peroxides formed on Tyr, *N*-Ac-Tyr, HPPA, and Gly-Tyr-Gly at 37°C indicated that the peroxides formed on HPPA and *N*-Ac-Tyr were the most stable, followed by those on Gly-Tyr-Gly and Tyr (Fig. 2b).

Photochemical stability of peroxides

Visible light illumination of preformed Tyr-derived peroxides, from which the RB had been removed, resulted in only minor peroxide loss (Fig. 2c). In contrast, exposure to broadband UV light resulted in rapid decomposition of the preformed peroxides, with almost complete loss observed after *ca* 90 min exposure (Fig. 2c).

Decomposition of peroxides by reductants

Treatment of photogenerated Tyr peroxides (*ca* 60 μ*M*) with Fe^{2+}–EDTA (a one-electron reducing system; 200 μ*M*) for 60 min at 4°C resulted in almost complete loss of the peroxides, as did treatment with sodium borohydride (a two-electron reductant; 200 μ*M*) (Fig. 2d).

Isolation of Tyr-derived peroxides and degradation products by HPLC

Reverse phase HPLC separation of photooxidized solutions of Tyr immediately after cessation of photolysis, using water (pH 7) as the mobile phase, gave two major product peaks eluting at retention times of 2.8 and 3.3 min, plus a peak from the parent amino acid at 6.1 min (Table 1). A somewhat greater resolution of these chromatograms was obtained using a mobile phase of 100 m*M* sodium perchlorate in sodium phosphate buffer at pH 2.5 (Fig. 3a). For reasons outlined subsequently, the peak eluting at 2.8 min is assigned to (**3**) and that eluting at 3.3 min to the peroxide (**1**). A further minor product that elutes at *ca* 4.7 min with water as the mobile phase (and 8.5 min using the perchlorate system) is assigned to 3,4-dihydroxyphenylalanine (DOPA) by comparison with authentic standards. No evidence was obtained for the presence of di-tyrosine. With increasing photolysis time before HPLC analysis the concentration of the parent Tyr peak decreased, and those assigned to (**1**) and (**3**) increased, with the former building up in a more rapid manner than the latter (Fig. 3a), consistent with these materials being photoproducts.

The relationship between these materials was studied in further experiments where the peak assigned to (**1**) was separated by HPLC and the collected fraction incubated for varying periods of time (up to 24 h) at 37°C, in the dark before reanalysis by HPLC (Fig. 3b). With increasing incubation time the peak assigned to (**1**) decreased in intensity, that assigned to (**3**) increased slowly, and a further intermediate that gave rise to a peak at *ca* 1.9 min was detected; this additional intermediate is assigned to the indolic peroxide (**2**). The time course of formation and decay of the species that give rise to these peaks is consistent with (**1**) being the precursor of (**2**), which, in turn, is the precursor of (**3**). The rate of decrease in intensity of the peak assigned to (**1**), as measured by HPLC peak area, correlates well with the loss of peroxide measured by the FOX assay. Absolute quantification of the yields of these intermediates proved to be impossible because of their short half-lives, which precluded the preparation of authentic standards.

Characterization of Tyr-derived peroxides and degradation products by MS

ESI-MS of the complete, nonfractionated, photolyzed reaction mixture gave both the molecular ion from the parent compound (as observed in control samples) and a further peak corresponding to M + 32; the latter was not detected in nonphotolyzed samples. The m/z value of this peak is consistent with the presence of two additional oxygen atoms, compared with the parent, and thus with the incorporation of a peroxide function. ESI-MS of the HPLC fraction assigned to (**1**) yielded an identical M + 32 peak. ESI-MS of the HPLC fraction assigned to (**3**) yielded a molecular ion with an m/z value of 198, corresponding to that expected for the M^+ ion of 3a-hydroxy-6-oxo-2,3,3a,6,7,7a-hexahydro-1*H*-indole-2-carboxylic acid (HOHICA).

Separation and characterization of peroxides derived from Tyr derivatives and Tyr-containing peptides

HPLC analysis of photolyzed solutions of HPPA gave rise to only a single peroxide-containing material as judged by

Table 1. Characteristics of photoproducts obtained from free Tyr, Tyr-containing peptides and related materials separated by HPLC*

Parent	Major product peaks and assignments			
	Product			
Free Tyr: retention time 6.1 min (14.6 min using perchlorate mobile phase)	Retention time ca 2 min Assignment: compound (**2**) Only seen upon further incubation of compound (**1**)	Retention time 3.3 min (3.8 min using perchlorate mobile phase) Assignment: compound (**1**) Test positive for peroxide using FOX assay m/z = 214† EPR signals identical to nonfractionated samples‡	Retention time 2.8 min (3.2 min using perchlorate mobile phase) Assignment: compound (**3**) Not peroxidic m/z = 198†	Retention time 4.7 min (8.5 min using perchlorate mobile phase) Assignment: DOPA
HPPA: retention time 34.5 min using perchlorate mobile phase (32.8 min using 0.1% TFA in water)	Not detected	Retention time 19.5 min using perchlorate mobile phase (18.3 min using 0.1% TFA in water) Assignment: compound (**5a**) Tests positive for peroxide using FOX assay m/z = 216 (Na adduct)† EPR signals identical to nonfractionated samples‡	Not detected	
N-Ac Tyr: retention time 4.5 min	Not detected	Retention time 2.3 min Tests positive for peroxide using FOX assay m/z = 278 (Na adduct)† EPR signals identical to nonfractionated samples‡	Not detected	
Gly-Tyr-Gly: retention time 23.0 min	Not detected	Retention time 5.5 min Tests positive for peroxide using FOX assay m/z = 328† EPR signals identical to nonfractionated samples‡	Not detected	

*HPLC was performed with a Zorbax ODS column at a flow rate of 1 mL min^{-1} with water as the mobile phase (unless stated otherwise) and the eluent monitored at 210 nm. Solutions containing 2.5 m*M* substrate and 10 μ*M* RB were photooxidized for 1 h using light from a Kodak S-AV 2050 slide projector with constant gassing with air at 4°C. See Materials and Methods for further details. Alternative mobile phases contained either 100 m*M* sodium perchlorate in 10 m*M* sodium phosphate buffer, pH 2.5 (perchlorate mobile phase), or 0.1% TFA in water.

†ESI-MS was performed on a VG Platform instrument using a 50% aqueous methanol–1% formic acid solvent system pumped at a flow rate of 10 μL min^{-1}; see Materials and Methods for further details.

‡EPR was performed on collected HPLC fractions with MNP (8.3 m*M*) and Fe^{2+}–EDTA (167 μ*M*, 1:1 complex) added and their EPR spectra recorded as described in the Materials and Methods section.

FOX assay, ESI-MS and the presence of EPR signals on treatment of the collected fractions with Fe^{2+}–EDTA in the presence of MNP (see following). The decay kinetics of the peroxide species present in the collected fraction matched that of the complete reaction mixture, and the EPR signals obtained from the fraction were identical to those from the unfractionated system (see following). Furthermore, the EPR parameters of the signals detected were similar, but not identical, to those detected with free Tyr. These data are consistent with similar peroxides and radicals being present in both cases. Similar analyses with *N*-Ac Tyr and Gly-Tyr-Gly confirmed the presence of analogous peroxides in these samples, which could be separated by HPLC and gave radicals on decomposition with Fe^{2+}–EDTA. These data are summarized in Table 1.

Characterization of Tyr-derived peroxides and degradation products by NMR

Examination by NMR of nonfractionated, photolyzed reaction mixtures containing free Tyr resulted in the detection of resonances consistent with the presence of HOHICA (**3**) and the indolic hydroperoxide (**2**) (Table 2). Both products were present as a mixture of two isomers in relative concentrations of ~1:1.5. The stereochemistry of each product was inferred from that of the reduction product of comparable concentration (see following). In both (**2**) and (**3**), the alpha-carbonyl protons, $H_{7\alpha}$ and $H_{7\beta}$, were almost fully exchanged with D_2O and the ^1H NMR resonances were correspondingly weak. No cross-peaks involving either of these protons were observed in NOESY spectra.

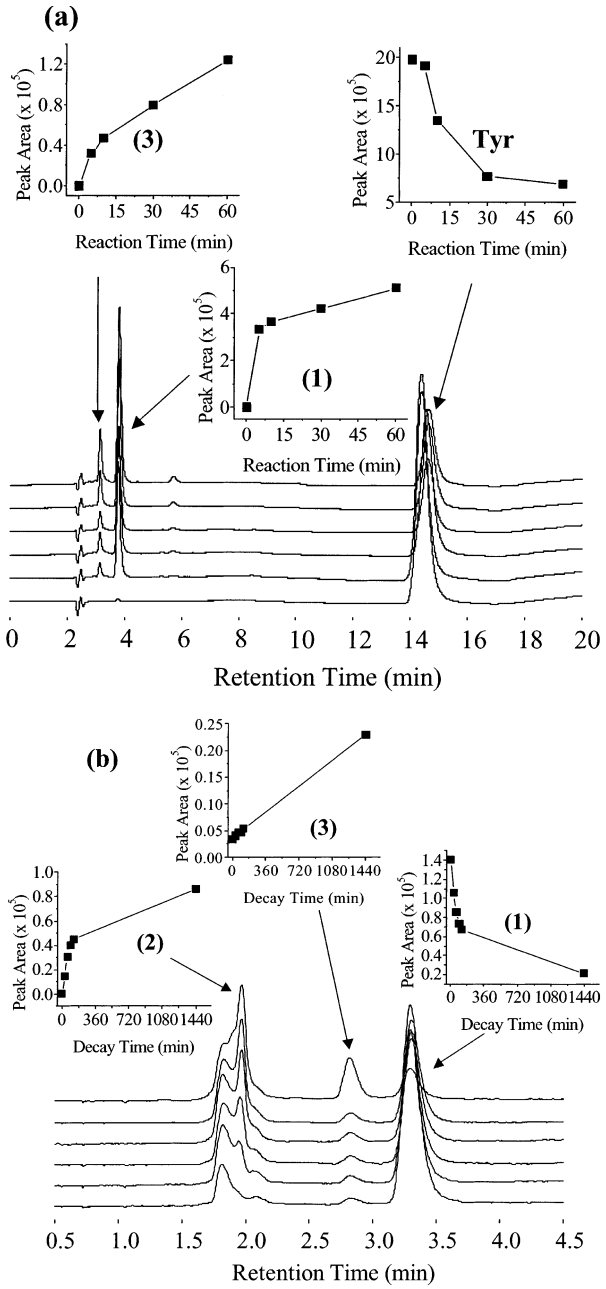

Figure 3. (a) HPLC analysis of Tyr oxidation products generated on photooxidation of free Tyr (2.5 m*M*) in D_2O in the presence of RB (10 μ*M*) for 1 h. Samples (10 μL) were removed at the indicated time points and injected onto a Zorbax ODS column. The mobile phase was 100 m*M* sodium perchlorate in 10 m*M* sodium phosphate buffer, pH 2.5. The elution rate was 1 mL min^{-1}, and the eluent was monitored at 210 nm. Insets show the rates of change of the various peak areas over the photooxidation period. (b) HPLC analysis of the time-dependent decay of the peak assigned to (**1**). The fraction assigned to (**1**) was collected from HPLC immediately after photooxidation and subsequently incubated at 37°C in the dark for periods of up to 24 h. At the indicated time points, samples were taken for reanalysis by HPLC. A Zorbax ODS column was used with water as the mobile phase. The elution rate was 1 mL min^{-1}, and the eluent was monitored at 210 nm. The peak at *ca* 1.7 min, which is constant in each trace, arises from the mobile phase. Insets show the rates of change of the various peak areas over the incubation period. See Materials and Methods for further details. Data from a single experiment, representative of several.

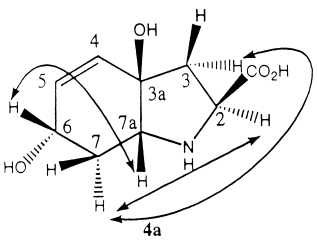

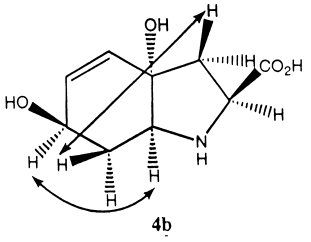

NMR examination (Table 2) of samples that had been photolyzed as described previously and then treated with $NaBH_4$ gave signals that are assigned to the corresponding allylic alcohols (**4a** and **4b**) arising from reduction of both the peroxide and carbonyl functions. In both compounds, there was some evidence of exchange of $H_{7\alpha}$ and $H_{7\beta}$ with D_2O, but the relative intensities of the ^1H resonances of these protons were much higher than those of the corresponding protons in HOHICA. For each of the diols, there were strong nuclear overhauser enhancement (NOE) cross-peaks between H_6 and H_{7a}, cross-peaks of slightly lower intensity between each pair of geminal protons ($H_{3\alpha}$–$H_{3\beta}$ and $H_{7\alpha}$–$H_{7\beta}$) and their vicinally coupled neighbours, and weak cross-peaks between the geminal protons in the five-membered ring and an olefinic proton. In addition, the major isomer showed a strong NOE cross-peak between one of the protons attached to C_7 and H_2 and a slightly weaker cross-peak between the same C_7 proton and one of the C_3 protons; for the minor isomer, there was a moderate intensity cross-peak between a C_7 and C_3 proton. The rationale for the assignments depicted on the structures is outlined subsequently.

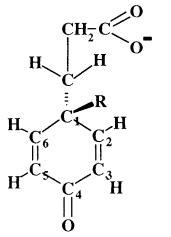

(**5a, R = OOH**)
(**5b, R = OH**)

(**6a, R = OOH**)
(**6b, R = OH**)

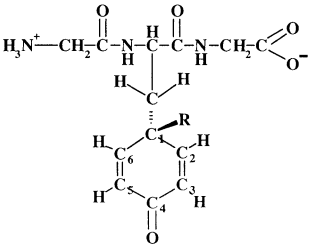

In contrast, NMR analysis of photooxidized HPPA (Table 3) immediately after cessation of photolysis indicated the formation of the hydroperoxide (**5a**). Reexamination of the NMR sample over a period of several months indicated slow decomposition of the hydroperoxide, accompanied by the appearance of resonances for the corresponding alcohol (**5b**) plus low concentrations of other materials that could not be definitively identified. The decay of this hydroperoxide, as evidenced by NMR, mirrored the slow decay observed by the FOX assay.

Table 2. NMR chemical shifts for (**2a**) and (**2b**), (2*S*, 3a*R*, 7a*R*)- and (2*S*, 3a*S*, 7a*S*)-3a-hydroperoxy-6-oxo-2,3,3a,6,7,7a-hexahydro-1*H*-indole-2-carboxylic acids, the corresponding 3a-alcohols, (**3a**) and (**3b**), and (**4a**) and (**4b**), (2*S*, 3a*R*, 6*S*, 7a*R*)- and (2*S*, 3a*S*, 6*R*, 7a*S*)-3a,6-dihydroxy-2,3,3a,6,7,7a-hexahydro-1*H*-indole-2-carboxylic acids

	Major OOH (**2a**)		Minor OOH (**2b**)		Major OH (**3a**)		Minor OH (**3b**)		Major diol (**4a**)		Minor diol (**4b**)	
Position	^{1}H	^{13}C	^{1}H	^{13}C	^{1}H	^{13}C	^{1}H	^{13}C	^{1}H	^{13}C	^{1}H	^{13}C
2	4.45	62.0	4.45	63.0	4.38	62.2	4.51	63.2	3.80	62.9	3.91	63.1
3α	2.82	39.2	2.86	39.1	2.79	42.6	2.77	42.4	2.40	45.9	2.33	45.3
3β	2.63		2.54		2.58		2.51		2.12		2.03	
3a		90.2		91.1		78.1		79.4		80.7		80.4
4	7.12	150.1	7.11	149.6	7.04	152.3	7.02	152.2	5.74	133.0	5.73	134.2
5	6.27	133.6	6.24	133.6	6.15	131.4	6.11	131.3	5.79	134.3	5.78	133.0
6		199.5		199.4		199.8		199.7	4.36	68.6	4.32	67.3
7α	3.07*	40.1	3.10*	40.2	3.01*	39.6	3.02*	40.3	1.47	38.3	2.17	37.3
7β	2.89*		2.90*		2.81*		2.83*		2.08		1.64	
7a	4.82	62.1	4.71	62.2	4.31	66.5	4.23	66.9	3.44	66.4	3.34	65.5
CO_2H		175.9		176.0		176.3		176.2		182.5		181.8

*Stereochemical assignment not determined.

Similarly, NMR analysis of photooxidized Gly-Tyr-Gly gave the hydroperoxide (**6a**), which decomposed over several months to the alcohol (**6b**) when the sample was kept at 5°C (Table 4). Samples of (**6a**) kept at 20°C decomposed relatively rapidly to yield comparatively complex NMR spectra, which could not be readily assigned; this is probably the result of the formation of multiple products *via* radical-mediated reactions (see subsequent discussion).

Peroxide formation by chemically generated $^1O_2$

Reaction of free Tyr, *N*-Ac-Tyr and Gly-Tyr-Gly with H_2O_2–MoO_4^{2-} gave substrate-derived peroxides as determined by HPLC separation and characterization of the resulting fractions as described previously. Similar fractions and retention times were detected on HPLC fractionation as in the RB experiments, though the extent of conversion of parent to products was greater; this presumably reflects a higher flux of $^1O_2$. Collection of the fraction corresponding to (**1**) and subsequent treatment with Fe^{2+}–EDTA in the presence of MNP gave EPR signals identical to those observed in the RB experiments (see following).

Free radical formation on decomposition of Tyr-derived peroxides

Experiments using thermal and visible light–induced decomposition of peroxides formed on free Tyr in the presence of either DMPO or MNP gave only weak radical adduct signals. This is probably because of a slow rate of radical formation under the conditions employed. In contrast, treatment of Tyr-derived peroxides (*ca* 125 μ*M* peroxide) with Fe^{2+}–EDTA (187.5 μ*M*, 1:1 complex) at pH 7.4 in the presence of the nitrone spin trap DMPO (187.5 m*M*) gave complex EPR signals (Fig. 4). Identical signals were detected with the HPLC fraction assigned to compound (**1**). These signals have been assigned to two different carbon-centered radical adducts plus DMPO–OH, on the basis of the measured hyperfine coupling constant (Table 5) and comparison with literature data (31). Experiments carried out under identical conditions with nonphotolyzed Tyr samples, or Tyr samples photolyzed in the absence of RB, did not give rise to any substrate-derived radical species.

Additional information on the nature of these species was obtained from experiments using the nitroso spin trap MNP, as this trap yields highly characteristic spectra with different carbon-centered radicals. Treatment of preformed Tyr peroxides (300 μ*M*) with Fe^{2+}–EDTA (167 μ*M*) in the presence

Table 3. NMR chemical shifts for (**5a**), 3-(1-hydroperoxy-4-oxo-2,5-cyclohexadien-1-yl)propionic acid and (**5b**), 3-(1-hydroxy-4-oxo-2,5-cyclohexadien-1-yl)propionic acid

	Hydroperoxide (**5a**)		Alcohol (**5b**)	
Position	^{1}H	^{13}C	^{1}H	^{13}C
1		84.5		72.4
2,5	7.09	153.9	7.01	155.9
3,6	6.41	133.3	6.27	130.5
4		191.2		191.4
CH_2 1′	2.03	33.8	2.08	37.5
CH_2 1″	2.14	33.7	2.14	33.6
CO_2H		183.2		183.5

Table 4. NMR chemical shifts for the hydroperoxide (**6a**) and alcohol (**6b**) formed on reaction of Gly-Tyr-Gly with singlet oxygen

	Hydroperoxide (**6a**)		Alcohol (**6b**)	
Position	^{1}H	^{13}C	^{1}H	^{13}C
HGly CH_2	3.74	43.2		
	3.84			
HGly CO		169.5		
CH	4.47	52.1	4.39	52.3
CH_2	2.22	40.0	2.25	43.9
	2.47		2.51	
Tyr*C1		82.9		71.1
Tyr*CH-2(6)	7.11	152.6	7.04	155.1
Tyr*CH-3(5)	6.39	132.8	6.23	129.7
Tyr*C-4		190.9		
Tyr*CH-5(3)	6.48	134.2	6.35	131.4
Tyr*CH-6(2)	7.12	153.0	7.05	154.6
CO		174.4		174.9
GlyOH CH_2	3.66	46.1	3.66	
	3.75		3.77	
CO_2H		179.1		

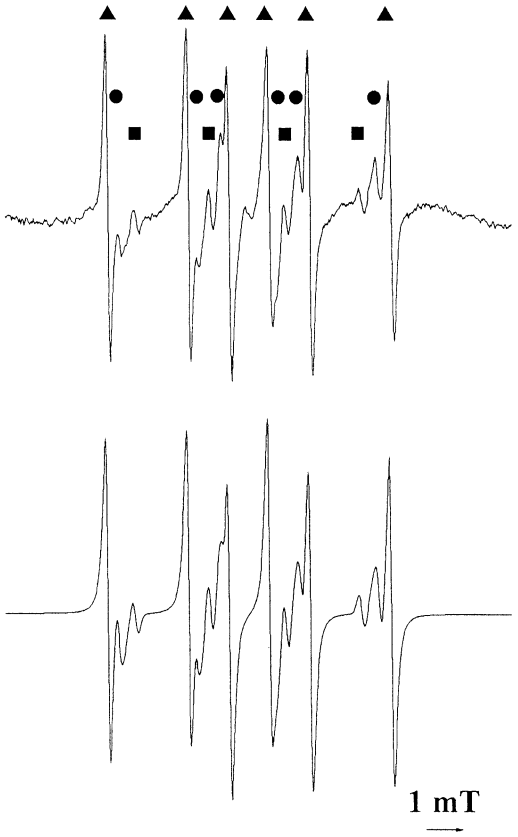

Figure 4. (a) EPR spectrum obtained on decomposition of Tyr-derived peroxides (*ca* 125 μ*M* peroxide) by Fe^{2+}–EDTA (187.5 μ*M*, 1:1 complex) in the presence of the spin trap DMPO (187.5 m*M*). Peroxides were generated and assayed as outlined in Fig. 1 and the Materials and Methods section. Spectrometer parameters were as follows: gain 5×10^5; modulation amplitude 0.05 mT; time constant 81 ms; scan time 42 s; center field 348 mT; field scan 10 mT; power 31.81 mW, with eight scans accumulated. Lines marked (■) are assigned to DMPO-OH, other lines are assigned to two carbon-centered radical adducts (▲, ●); see text and Table 5 for further details. (b) Computer simulation of the spectrum in (a) using the parameters given in Table 5.

of MNP (8.3 m*M*) at pH 7.4 resulted in the detection of EPR signals that have been assigned, on the basis of their hyperfine coupling constants, to two different carbon-centered species and the spin trap degradation product di-*tert*-butylnitroxide. The splitting patterns of these signals are consistent with the trapping of radicals with partial structure ·CHRR′ and ·CH(R)CHR′R″, *i.e.* with one and two neighboring protons, respectively (Table 5, Fig. 5a). Experiments carried out in a manner identical to those described previously but with peroxides generated from Tyr deuterated at the C(3) (methylene, -CH_2-) position gave spectra identical to the nonlabeled substrate, eliminating this position as the site of the observed radicals. In contrast, experiments with Tyr deuterated at the 3,5 ring positions resulted in a change in the spectra of both the radical signals observed with nonlabeled Tyr, consistent with both radicals having couplings to the hydrogen atom (or deuterium) at the ring 3,5 positions (Fig. 5c). Similar experiments with Tyr deuterated at all available ring positions (2,3,5,6) resulted in a further simplification of the spectra, consistent with the presence of at least one further small coupling to the 2 (or 6) position (Fig. 5d).

Analogous experiments with photooxidized HPPA, *N*-Ac-Tyr and Gly-Tyr-Gly (both unfractionated reaction mixtures, or the peroxide-containing HPLC fractions) gave similar EPR signals, and these spectra are likewise assigned to ring-derived, carbon-centered radicals (Table 5).

Treatment of photooxidized BSA (*ca* 200 μ*M* peroxide) with Fe^{2+}–EDTA (167 μ*M*, 1:1 complex) in the presence of MNP (8.3 m*M*) gave broad EPR signals assigned to large, slowly tumbling, protein-derived spin adducts (Fig. 6a). Further information regarding the nature of these species was obtained by digestion of these long-lived adducts with pronase (2 units, 15 min, 37°C), which results in the release of low molecular weight fragments that still have the spin trap attached (32,33). Subsequent EPR analysis of this material showed the presence of a number of spin adducts, with some of the observed features having coupling constants similar to those detected with free Tyr and Tyr-containing peptides (Fig. 6b, *cf.* Fig. 5a). The similarity between these features is consistent with, but does not prove, the formation of similar Tyr-derived peroxides and radicals on photooxidized proteins.

DISCUSSION

Previous studies of the reaction of $^1O_2$ with free Tyr have provided evidence for the formation of the cyclized indolic material HOHICA (17–19). This material has been suggested to arise *via* the reactions illustrated in Scheme 1. We, and others, have previously provided evidence for the formation of peroxides as intermediates in such reactions with free Tyr (17,18,33), though the exact nature of these materials, and their subsequent reactions, have not been studied in detail.

In the present study, the formation and subsequent decay of peroxides formed on exposure of free Tyr and Tyr-containing peptides and proteins to visible light in the presence of RB, or a molybdate–H_2O_2 system, have been examined. The yield of peroxides formed was enhanced in the presence of D_2O, and decreased by azide, consistent with the intermediacy of $^1O_2$. No evidence has been obtained, by HPLC analysis, for the formation of significant yields of DOPA or di-tyrosine, which are characteristic markers of oxidation of Tyr by HO· and other radical oxidants (34), suggesting that these reactions are predominantly nonradical in nature. These observations are in accord with a previous report (35). The absence of peroxides in control experiments with the Tyr-containing materials and with photolyzed Gly-Gly-Gly indicates that the peroxides are not generated by direct photooxidation or as a result of ''dark'' (nonphotolytic) reactions and that these peroxides are generated on the aromatic ring of Tyr.

The analytical data obtained with free Tyr are consistent with the presence of two peroxide species (**1**) and (**2**) (Scheme 1). The time course of loss of the parent amino acid and formation of these species suggests that the postulated endoperoxide precursor (see Scheme 1) is very short-lived and only ever present at low concentrations. This is in accord with previous reports on related materials (36,37). The intermediate (**1**) reacts relatively rapidly with the amine group of the free amino acid to give the ring-closed hydro-

Table 5. EPR parameters of spin adducts formed on reaction of Fe^{2+}–EDTA with peroxides formed on RB-mediated photooxidation of free Tyr and related compounds*

Substrate	Spin trap	Hyperfine coupling constants† (mT) a(N)	a(H)	a(H)	Assignment
Tyr	DMPO	1.60	2.41		Ring-derived radical
		1.54	2.06		Ring-derived radical
		1.49	1.49		DMPO–OH
Tyr	MNP	1.50	0.21		Ring-derived radical
		1.59	0.13		Ring-derived radical
(3,5-ring-d_2)-Tyr	MNP	1.51			Ring-derived radical
		1.59			Ring-derived radical
(2,3,5,6-ring-d_4)-Tyr	MNP	1.51			Ring-derived radical
		1.59			Ring-derived radical
HPPA	MNP	1.53	0.21		Ring-derived radical
		1.54	0.16		Ring-derived radical
		1.53	0.22	0.08	Ring-derived radical
N-Ac Tyr	MNP	1.50	0.19		Ring-derived radical
		1.57	0.23		Ring-derived radical
Gly-Tyr-Gly	MNP	1.52	0.23		Ring-derived radical
		1.54	0.13		Ring-derived radical

*Free Tyr and related compounds (each 2.5 m*M*) were exposed to visible light for 1 h in the presence of 10 μ*M* RB at 4°C with constant aeration. After treatment with catalase to remove H_2O_2 (see Materials and Methods) the resulting peroxides were treated with Fe^{2+}–EDTA (167 μ*M*, 1:1 complex) in the presence of MNP (8.3 m*M*) and EPR spectra recorded as described in the Materials and Methods.
†Error in hyperfine coupling constants is estimated to be ±0.02 mT.

peroxide species (**2**), which has been separated by HPLC and fully characterized by NMR. No peaks that could be assigned to (**1**) were detected by NMR; this is likely to be because of the rapid conversion of this material into (**2**). The peroxide (**2**) subsequently decays, *via* a non-radical mechanism, to give the stable alcohol (**3**), which has been identified by NMR and MS as HOHICA. Because these peroxides account for nearly 100% of the products obtained from free Tyr, and (**2**) appears to convert cleanly (as judged by the absence of other significant NMR signals) into HOHICA, the latter is confirmed as the major $^1O_2$-mediated photooxidation product of free Tyr. Although it has been reported that HOHICA can be oxidized further, under alkaline conditions, to give rise to a decarboxylated keto compound (*cf.* Scheme 1) (17,19), no evidence for the formation of this species was detected in the present studies. This may be because of the short reaction times and the neutral pH conditions employed here.

The hydroperoxides (**2**) were readily distinguishable from HOHICA by comparison of the chemical shifts for C_{3a} with literature data (38). The NMR data reported here suggest that each compound was present as a mixture of two isomers. Both *cis* (18) and *trans* (17) ring junctions have previously been suggested for HOHICA. NOESY spectra of the HOHICA/hydroperoxide mixture confirmed the stereochemical relationships in the five-membered ring, on the basis of the reasonable assumption (supported by models) that the relative intensities of NOE between the H_2 and respective H_3 protons would be similar to those observed for proline residues in proteins (39), but no useful NOE involving the six-membered rings were observed.

The stereochemical assignments for (**2**) and (**3**) were thus established indirectly. Sodium borohydride reduction of the photolysis mixture containing (**1**)–(**3**) yielded a mixture of allylic alcohols (**4a** and **4b**). For each isomer, the NOE cross-peaks between the respective proton derived from borohydride (H_6) and ring junction proton (H_{7a}) indicate that the reduction of the carbonyl groups was stereoselective, presumably directed by initial complexation of borohydride with the oxygen at C_{3a} (40). Models show that for a *trans* ring-junction, all reasonable conformations place H_{7a} even closer to the *cis* proton attached to C_3 than to H_6, yet there was no evidence of an NOE cross-peak between H_{7a} and either of the C_3 protons. Further, internuclear distances for the through-space correlations indicated on the structures are significantly shorter for the *cis* ring junction than for the corresponding molecules with a *trans* ring junction. In the absence of comparative data, the latter cannot be totally excluded, but the *cis* stereochemistry, which is mechanistically favored (18), appears more likely. Because the isomeric allylic alcohols were obtained in proportions similar (unequal) to that observed for HOHICA and its precursor hydroperoxides, the stereochemistry of the ring junction for the ketones can be inferred from that of the characterized allylic alcohols.

Photooxidation of HPPA, which lacks the free amine group, gave rise to the peroxide (**5a**), which has been previously reported as an intermediate in the photooxygenation of HPPA under alkaline conditions (41,42), whereas photooxidation of Gly-Tyr-Gly led to the analogous peroxide (**6a**). These compounds have both been fully characterized by NMR and yield similar spectra, except for the extended influence of chirality on chemical shifts in (**6**). The enhanced stability of (**5a**) compared with (**1**) is consistent with the hypothesis that reaction with the amine group is a major pathway to removal of (**1**). The hydroperoxides (**5a**) and (**6a**) decay slowly, at low temperatures, to the corresponding alcohols (**5b**) and (**6b**), as evidenced by their behavior on HPLC, and analysis by NMR and MS. The concentration of (**6b**) was sufficient to enable full assignment of the HSQC spectrum but insufficient to provide all anticipated HMBC cross-peaks, even in experiments using a total acquisition

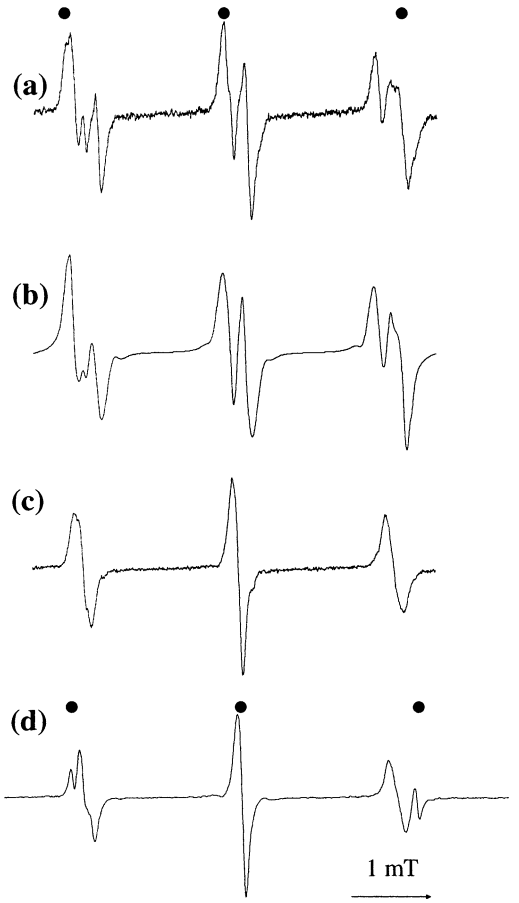

Figure 5. (a) EPR spectrum observed on reaction of Tyr-derived peroxides (*ca* 300 μ*M* peroxide) with Fe^{2+}–EDTA (167 μ*M*, 1:1 complex) in the presence of MNP (8.3 m*M*). (b) Computer simulation of the spectrum in (a) using the parameters in Table 5. (c) As (a), except with peroxides generated on 3,5-ring-d_2-Tyr. (d) As (a), except with peroxides generated on 2,3,5,6-ring-d_4-Tyr. Peroxides were generated and assayed as described in Fig. 1 and the Materials and Methods section. Spectrometer parameters were as follows: gain 5×10^5; modulation amplitude 0.005 mT; time constant 81 ms; scan time 84 s; center field 348 mT; field scan 4 mT; power 31.81 mW, with four scans accumulated. Lines marked (●) are assigned to di-*tert*-butyl-nitroxide, other lines are assigned to carbon-centered radical adducts; see text and Table 5 for further details.

time of >70 h. Nevertheless, the spectral data, and especially the chemical shifts of the oxygenated carbons (C_1), are sufficiently comparable in the pairs of products (**5b**) and (**6b**) to support the conclusion that decompositions of (**5a**) and (**6a**) occur in a comparable manner at 5°C.

The absence of a cyclization reaction with the peroxide (**6a**) derived from Gly-Tyr-Gly, to give species analogous to (**2**), is as expected, as this process should be slowed down by the delocalization of the nitrogen lone pair into the peptide bond, making this atom a less efficient nucleophile for the Michael reaction, which results in ring-closure. Thus peroxides analogous to (**6a**) and the corresponding alcohol (**6b**), rather than (**2**) and (**3**), would be predicted to be the major species generated on $^1O_2$-mediated oxidation of Tyr residues in proteins. A cyclized species analogous to (**2**) has, however, been detected as a product of the $^1O_2$-mediated photooxidation of *N*-acetyltyramine (41). This oxidation was, however, carried out under alkaline conditions (pH 8.7) that

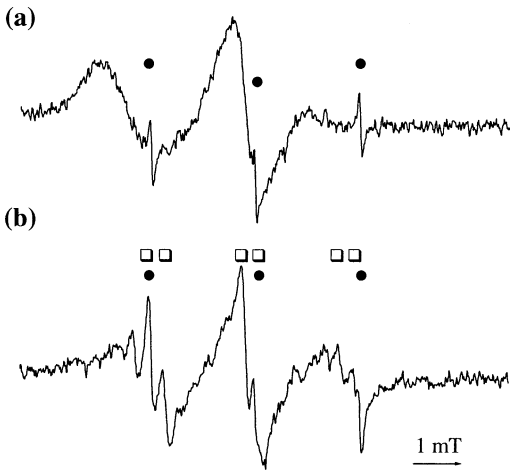

Figure 6. (a) EPR spectrum observed on reaction of BSA-derived peroxides (*ca* 200 μ*M* peroxide) with Fe^{2+}–EDTA (167 μ*M*, 1:1 complex) in the presence of MNP (8.3 m*M*). (b) As (a), except after incubation of the preformed adducts with pronase (2 units, 15 min, 37°C). Peroxides were generated and assayed as described in Fig. 1 and the Materials and Methods section. Spectrometer parameters were as follows: gain 1×10^6; modulation amplitude 0.2 mT; time constant 81 ms; scan time 42 s; center field 348 mT; field scan 8 mT; power 31.81 mW, with eight scans accumulated. Lines marked (●) are assigned to di-*tert*-butyl-nitroxide, those marked (□) are assigned to carbon-centered radical adducts derived from Tyr-derived peroxides; see text and Table 5 for further details.

might encourage the formation of the ring-closed species. Studies to confirm the nature of the products formed as a result of the photooxidation of Tyr residues on proteins are currently underway.

All of these peroxides are unstable and decompose at temperatures above 4°C, with the rate of decay increased at elevated temperatures, consistent with thermal breakdown. Decomposition of these peroxides occurs rapidly in the presence of metal ions, $NaBH_4$ and UV light; in contrast, visible light in the absence of a sensitizer has only marginal effects.

In the case of decomposition induced by metal ions or UV light, reactive free radicals have been detected by EPR spin trapping. In each case, the experimental hyperfine coupling constants of these adducts are consistent with the formation of ring-derived radicals obtained from further reaction of the initial, undetected, alkoxyl radicals. These alkoxyl radicals are believed to be generated from (**1**) and (**2**), and analogous species, by a pseudo-Fenton reaction (*i.e.* reactions A in Scheme 2; *cf.* data on the decomposition of other amino acid–, peptide- and protein-bound peroxides [43,44]). Subsequent reaction of such alkoxyl radicals with the neighboring double bond results in the formation of carbon-centered radicals at the 3 (or 5) position on the aromatic ring *via* epoxide formation (reactions B, Scheme 2), which are subsequently trapped with MNP or DMPO. The assignment of these species as intermediates generated from (**1**) or (**2**) in the case of free Tyr, and (**5a**) and (**6a**) from HPPA and Gly-Tyr-Gly, respectively, is consistent with the detection of identical signals from the HPLC fractions and the complete reaction mixtures.

Alkoxyl radical addition to neighboring double bonds is particularly rapid, and a major reaction pathway for alkoxyl radicals formed during the decomposition of unsaturated fat-

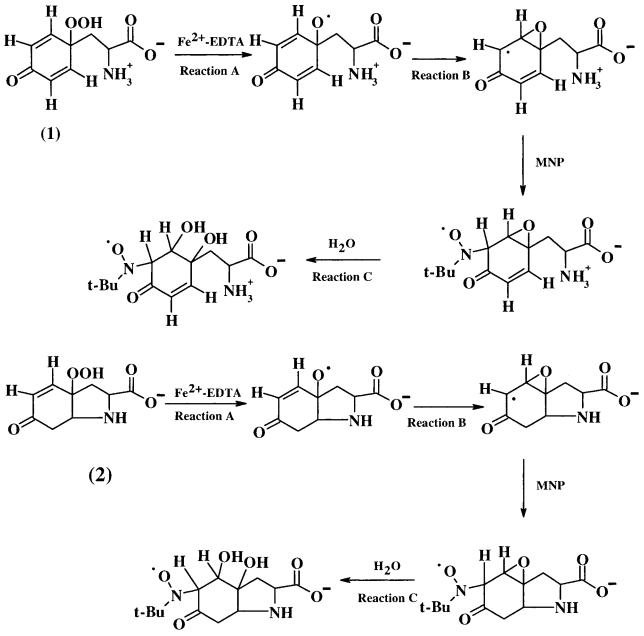

Scheme 2.

ty acid hydroperoxides (45). The detection of significant spectral changes for both radical adducts on use of the 3,5-ring-d_2 Tyr is consistent with both species being centered at the 3 (or 5) position. However, the additional differences between the adducts detected from 3,5-ring-d_2 Tyr and 2,3,5,6-ring-d_4 Tyr suggest that the second radical species—that which has two proton couplings—is a C_3–C_5–centered radical, with the second smaller coupling arising from C_2 (or C_6). This second species is assigned to a radical adduct derived from the initial epoxide as a result of hydrolytic ring opening (*i.e.* reaction C, Scheme 2).

In conclusion, it has been demonstrated that $^1O_2$-mediated oxidation of free Tyr gives rise to multiple intermediate peroxides including two isomers of (**2**), presumably *via* the intermediacy of (**1**), and that these species undergo thermal decay to give two isomers of the ring-closed indolic alcohol HOHICA. These species have been characterized in detail. In contrast, *N*-protected tyrosine derivatives, and Tyr residues in peptides, give rise to long-lived, ring-derived hydroperoxides with the peroxide function present at the C_1 ring position. These materials have been fully characterized by NMR and are the likely $^1O_2$-mediated oxidation products of Tyr residues on proteins. At low temperatures these hydroperoxides decay to the corresponding alcohols, which may be suitable markers of $^1O_2$-mediated oxidation of Tyr residues on proteins. At physiological temperatures, and particularly in the presence of UV light or metal ions, these hydroperoxides can give rise to further reactive radicals. Both the parent hydroperoxides, and radicals derived from them, may mediate further oxidative damage. Initial studies (23) have shown that these species can inhibit key cellular enzymes. The formation and subsequent reactions of $^1O_2$-mediated protein peroxides may therefore play a key role in the damage induced by UV light and other sources of $^1O_2$.

Acknowledgments—The authors thank the Australian Research Council and the Wellcome Trust for financial support. A.W. acknowledges the receipt of an Australian Postgraduate Award administered through the University of Sydney.

REFERENCES

1. Kanofsky, J. R. (1983) Singlet oxygen production by lactoperoxidase. *J. Biol. Chem.* **258**, 5991–5993.
2. Kanofsky, J. R., J. Wright, G. E. Miles-Richardson and A. I. Tauber (1984) Biochemical requirements for singlet oxygen production by purified human myeloperoxidase. *J. Clin. Investig.* **74**, 1489–1495.
3. Kanofsky, J. R. and B. Axelrod (1986) Singlet oxygen production by soybean lipoxygenase isozymes. *J. Biol. Chem.* **261**, 1099–1104.
4. Kanofsky, J. R., H. Hoogland, R. Wever and S. J. Weiss (1988) Singlet oxygen production by human eosinophils. *J. Biol. Chem.* **20**, 9692–9696.
5. Steinbeck, M. J., A. U. Khan and M. J. Karnovsky (1992) Intracellular singlet oxygen generation by phagocytosing neutrophils in response to particles coated with a chemical trap. *J. Biol. Chem.* **267**, 13425–13433.
6. Steinbeck, M. J., A. U. Khan and M. J. Karnovsky (1993) Extracellular production of singlet oxygen by stimulated macrophages quantified using 9,10-diphenylanthracene and perylene in a polystyrene film. *J. Biol. Chem.* **268**, 15649–15854.
7. Bensasson, R. V., E. J. Land and T. G. Truscott (1993) *Excited States and Free Radicals in Biology and Medicine.* Oxford University Press, Oxford.
8. Plesnicar, B. (1992) Polyoxides. In *Organic Peroxides,* (Edited by W. Ando), pp. 479–533. John Wiley and Sons, Chichester.
9. Straight, R. C. and J. D. Spikes (1985) Photosensitized oxidation of biomolecules. In *Singlet O_2,* Vol. 4 (Edited by A. A. Frimer), pp. 91–143. CRC Press, Boca Raton.
10. Tyrrell, R. M. (2000) Role for singlet oxygen in biological effects of ultraviolet A radiation. *Methods Enzymol.* **319**, 290–296.
11. Giacomoni, P. U. (Editor)(2001) *Sun Protection in Man.* Elsevier, Amsterdam.
12. Davies, M. J. and R. J. W. Truscott (2001) Photo-oxidation of proteins and its consequences. In *Sun Protection in Man,* (Edited by P. U. Giacomoni), pp. 251–275. Elsevier, Amsterdam.
13. Matheson, I. B. C., R. D. Etheridge, N. R. Kratowich and J. Lee (1975) The quenching of singlet oxygen by amino acids and proteins. *Photochem. Photobiol.* **21**, 165–171.
14. Michaeli, A. and J. Feitelson (1994) Reactivity of singlet oxygen toward amino acids and peptides. *Photochem. Photobiol.* **59**, 284–289.
15. Wilkinson, F., W. P. Helman and A. B. Ross (1995) Rate constants for the decay and reactions of the lowest electronically excited state of molecular oxygen in solution. An expanded and revised compilation. *J. Phys. Chem. Ref. Data* **24**, 663–1021.
16. Papeschi, G., M. Monici and S. Pinzauti (1982) pH effect on dye sensitized photooxidation of aminoacids and albumins. *Med. Biol. Environ.* **10**, 245–250.
17. Endo, K., K. Seya and H. Hikino (1988) Photo-oxidation of L-tyrosine, an efficient, 1,4-chirality transfer reaction. *J. Chem. Soc. Chem. Commun.* 934–935.
18. Jin, F. M., J. Leitich and C. von Sonntag (1995) The photolysis (λ = 254 nm) of tyrosine in aqueous solutions in the absence and presence of oxygen—the reaction of tyrosine with singlet oxygen. *J. Photochem. Photobiol. A Chem.* **92**, 147–153.
19. Criado, S., A. T. Soltermann, J. M. Marioli and N. A. Garcia (1998) Sensitized photooxidation of di- and tripeptides of tyrosine. *Photochem. Photobiol.* **68**, 453–458.
20. Roberts, J. E. (2001) Hazards of sunlight exposure in the eye. In *Sun Protection in Man,* (Edited by P. U. Giacomoni), pp. 155–174. Elsevier, Amsterdam.
21. Sysak, P. K., C. S. Foote and T.-Y. Ching (1977) Chemistry of singlet oxygen—XXV. Photooxygenation of methionine. *Photochem. Photobiol.* **26**, 19–27.
22. Straight, R. C. and J. D. Spikes (1978) Sensitized photooxygenation of amino acids: effects on the reactvity of their primary amine groups with fluorescamine and O-phthalaldehyde. *Photochem. Photobiol.* **27**, 565–569.

23. Morgan, P. E., R. T. Dean and M. J. Davies (2002) Inhibition of glyceraldehyde-3-phosphate dehydrogenase by peptide and protein peroxides generated by singlet oxygen attack. *Eur. J. Biochem.* **269,** 1916–1925.
24. Fu, S., S. Gebicki, W. Jessup, J. M. Gebicki and R. T. Dean (1995) Biological fate of amino acid, peptide and protein hydroperoxides. *Biochem. J.* **311**, 821–827.
25. Gebicki, S., R. T. Dean and J. M. Gebicki (1996) Inactivation of glutathione reductase by protein and amino acid peroxides. In *Oxidative Stress and Redox Regulation: Cellular signalling, AIDS, Cancer and Other Diseases,* p. 139. Institute Pasteur, Paris.
26. Gebicki, S. and J. M. Gebicki (1999) Crosslinking of DNA and proteins induced by protein hydroperoxides. *Biochem. J.* **338**, 629–636.
27. Luxford, C., B. Morin, R. T. Dean and M. J. Davies (1999) Histone H1- and other protein- and amino acid-hydroperoxides can give rise to free radicals which oxidize DNA. *Biochem. J.* **344**, 125–134.
28. Luxford, C., R. T. Dean and M. J. Davies (2000) Radicals derived from histone hydroperoxides damage nucleobases in RNA and DNA. *Chem. Res. Toxicol.* **13**, 665–672.
29. Spector, A., G. M. Wang, R. R. Wang, W. C. Li and N. J. Kleiman (1995) A brief photochemically induced oxidative insult causes irreversible lens damage and cataract. II. Mechanism of action. *Exp. Eye Res.* **60**, 483–493.
30. Gay, C., J. Collins and J. M. Gebicki (1999) Hydroperoxide assay with the ferric-xylenol orange complex. *Anal. Biochem.* **273**, 149–155.
31. Buettner, G. R. (1987) Spin trapping: ESR parameters of spin adducts. *Free Radic. Biol. Med.* **3**, 259–303.
32. Davies, M. J., B. C. Gilbert and R. M. Haywood (1991) Radical-induced damage to proteins: e.s.r. spin-trapping studies. *Free Radic. Res. Commun.* **15**, 111–127.
33. Wright, A., C. L. Hawkins and M. J. Davies (2000) Singlet oxygen-mediated protein oxidation: evidence for the formation of reactive peroxides. *Redox Rep.* **5**, 159–161.
34. Davies, M. J., S. Fu, H. Wang and R. T. Dean (1999) Stable markers of oxidant damage to proteins and their application in the study of human disease. *Free Radic. Biol. Med.* **27**, 1151–1163.
35. Balasubramanian, D., X. Du and J. S. J. Zigler (1990) The reaction of singlet oxygen with proteins, with special reference to crystallins. *Photochem. Photobiol.* **52**, 761–768.
36. Kang, P. and C. S. Foote (2000) Synthesis of a C-13, N-15 labeled imidazole and characterization of the 2,5-endoperoxide and its decomposition. *Tetrahedron Lett.* **41**, 9623–9626.
37. Takabatake, T., T. Miyazawa, M. Hasegawa and C. S. Foote (2001) Reaction of 4,7-dimethylbenzofurazan with singlet oxygen. *Tetrahedron Lett.* **42**, 987–989.
38. Sy, L.-K., S.-M. Hui, K.-K. Cheung and G. D. Brown (1997) A rearranged hydroperoxide from the reduction of artemisinin. *Tetrahedron* **53**, 7493–7500.
39. Cai, M., Y. Huang, J. Liu and R. Krishnamoorthi (1995) Solution conformations of proline rings in proteins studied by NMR spectroscopy. *J. Biomol. NMR* **6**, 123–128.
40. Fessenden, R. J. and J. S. Fessenden (1990) *Organic Chemistry*, Brooks/Cole Publishing Company, Pacific Grove, California.
41. Saito, I., Y. Chujo, H. Shimazu, M. Yamane, T. Matsuura and H. J. Cahnmann (1975) Nonenzymic oxidation of *p*-hydroxyphenylpyruvic acid with singlet oxygen to homogentisic acid. A model for the action of *p*-hydroxyphenylpyruvate hydroxylase. *J. Am. Chem. Soc.* **97**, 5272–5277.
42. Saito, I., M. Yamane, H. Shimazu, T. Matsuura and H. J. Cahnmann (1975) Biogenetic type conversion of *p*-hydroxyphenylpyruvic acid into homogentisic acid. *Tetrahedron Lett.* **9**, 641–644.
43. Davies, M. J., S. Fu and R. T. Dean (1995) Protein hydroperoxides can give rise to reactive free radicals. *Biochem. J.* **305**, 643–649.
44. Davies, M. J. (1996) Protein and peptide alkoxyl radicals can give rise to C-terminal decarboxylation and backbone cleavage. *Arch. Biochem. Biophys.* **336**, 163–172.
45. Wilcox, A. L. and L. J. Marnett (1993) Polyunsaturated fatty acid alkoxyl radicals exist as carbon-centered epoxyallylic radicals: a key step in hydroperoxide-amplified lipid peroxidation. *Chem. Res. Toxicol.* **6**, 413–416.